Ecotoxicology and Environmental Safety 263 (2023) 115356

Contents lists available at ScienceDirect

Ecotoxicology and Environmental Safety

journal homepage: www.elsevier.com/locate/ecoenv

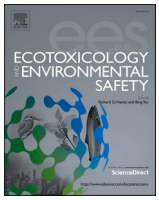

Microglia-derived exosomal circZNRF1 alleviates paraquat-induced neuronal cell damage via miR-17-5p

Xu Liu [a,b,1], Qingqing Wu [a,b,1], Jingwen Wu [a,b], Jianxi Liu [e], Fuli Zheng [a,b,c], Guangxia Yu [a,b,c], Hong Hu [a,b,c], Zhenkun Guo [a,b], Siying Wu [a,c,d], Huangyuan Li [a,b,c,*], Wenya Shao [a,b,c,*]

[a] Fujian Provincial Key Laboratory of Environmental Factors and Cancer, School of Public Health, Fujian Medical University, Fuzhou 350122, China
[b] Department of Preventive Medicine, School of Public Health, Fujian Medical University, Fuzhou 350122, China
[c] The Key Laboratory of Environment and Health, School of Public Health, Fujian Medical University, Fuzhou 350122, China
[d] Department of Epidemiology and Health Statistics, School of Public Health, Fujian Medical University, Fuzhou 350122, China
[e] College of Environmental and Resource Sciences, College of Carbon Neutral Modern Industry, Fujian Key Laboratory of Pollution Control & Resource Reuse, Fujian Normal University, Fuzhou 350007, China

ARTICLE INFO

Edited by Professor Bing Yan

Keywords:
Exosome
Circular RNA
Apoptosis
Parkinson's disease
Paraquat

ABSTRACT

Paraquat (PQ) is an environmental poison that causes clinical symptoms similar to those of Parkinson's disease (PD) *in vitro* and in rodents. It can lead to the activation of microglia and apoptosis of dopaminergic neurons. However, the exact role and mechanism of microglial activation in PQ-induced neuronal degeneration remain unknown. Here, we isolated the microglia-derived exosomes exposed with 0 and 40 μM PQ, which were subsequently co-incubated with PQ-exposed neuronal cells to simulate intercellular communication. First, we found that exosomes released from microglia caused a change in neuronal cell vitality and reversed PQ-induced neuronal apoptosis. RNA sequencing data showed that these activated microglia-derived exosomes carried large amounts of circZNRF1. Moreover, a bioinformatics method was used to study the underlying mechanism of circZNRF1 in regulating PD, and miR-17–5p was predicted to be its target. Second, an increased Bcl2/Bax ratio could play an anti-apoptotic role. Bcl2 was predicted to be a downstream target of miR-17–5p. Our results showed that circZNRF1 plays an anti-apoptotic role by absorbing miR-17–5p and regulating the binding of Bcl2 after exosomes are internalized by dopaminergic neurons. In conclusion, we demonstrated a new intercellular communication mechanism between microglia and neurons, in which circZNRF1 plays a key role in protecting against PQ-induced neuronal apoptosis through miR-17–5p to regulate the biological process of PD. These findings may offer a novel approach to preventing and treating PD.

1. Introduction

Paraquat (PQ) is widely used owing to its high weeding efficiency and low cost. PQ is associated with several neurodegenerative diseases; however, the underlying pathogenesis of PQ-induced neurodegenerative injury remains controversial (Huang et al., 2019; Stuart et al., 2023; Verssimo et al., 2017; Zhang et al., 2016). Chronic low-level doses of PQ exposure, such as in farm workers and people living near pesticide use or production sites, increase the incidence rate of central nervous system degenerative diseases (e.g., Parkinson's disease (PD)) (Ahmed et al.,

Abbreviations: PQ, Paraquat; PD, Parkinson's disease; CircZNRF1, Circular RNA circZNRF1; MiR-17–5p, MicroRNA-17–5p; Bcl2, B cell lymphoma/leukemia 2; MPTP, 1-Methyl-4-phenyl-1,2,3,6-tetrahydropyridine; MPP^+, 1-Methyl-4-phenylpyridinium ion; VdFBS, Vesicle-depleted fetal bovine serum; EV, Extracellular vesicle; Ctrl-EXO, Control group exosomes; PQ-EXO, PQ group exosomes; TEM, Transmission electron microscope; NTA, Nanoparticle tracking analysis; TSG101, Endosomal sorting complex required for transport-I complex subunit; CD63 and CD81, Cluster of differentiation 63 and 81 proteins; Bax, B cell lymphoma/leukemia 2 associated X protein; GAPDH, Glyceraldehyde-3-phosphate dehydrogenase; Caspase, Cysteinyl aspartate specific proteinase; GO, Gene ontology; KEGG, Kyoto encyclopedia of genes and genomes; ROS, Reactive oxygen species; EDTA, Ethylene diamine tetraacetic acid; PI3K, Phosphatidylinositol3-kinase; AKT, Protein kinase B; AMPK, Adenosine 5'-monophosphate (AMP)-activated protein kinase; mTOR, Mammalian target of rapamycin; FoxO, Forkhead box O; IL-6, interleukin 6.

* Corresponding authors at: Fujian Provincial Key Laboratory of Environmental Factors and Cancer, School of Public Health, Fujian Medical University, Fuzhou 350122, China.
E-mail addresses: fmulhy@163.com (H. Li), shaowenya@yeah.net (W. Shao).
[1] Authors contributed equally to this article.

https://doi.org/10.1016/j.ecoenv.2023.115356
Received 12 April 2023; Received in revised form 19 July 2023; Accepted 9 August 2023

2017). Previously, we found that apoptosis increased and dopaminergic neurons were significantly reduced ($P < 0.05$) in a PQ-exposed mouse model (Wang et al., 2017). The main event in the neuroinflammatory reactions in the brain is microglial activation, which plays an essential role in the development and occurrence of PD (Cheng et al., 2020; Qiao et al., 2022; Shi et al., 2019). A large number of activated microglia have been observed in mouse models of PD exposed to MPTP (a PQ analog) over an extended period (Tangamornsuksan et al., 2019). This indicates that environmental chemical poisons may be involved in the occurrence and development of PD through the abnormal activation of microglia, which can increase the apoptosis of dopaminergic neurons induced by MPP^+ (Peng et al., 2019). Although microglia can enhance PD progression in toxic environments, whether coordination between microglia and dopaminergic neurons is involved in this process remains unknown.

Exosomes allow biological molecules (including nucleic acids and proteins) to be transported to distant cells to perform their corresponding biological functions (Bliederhaeuser et al., 2016; Kalluri and LeBleu, 2020). Glial cellular exosomes can affect the physiological and pathological functions of neurons (Chamberlain et al., 2021; Fan et al., 2022). The activated microglia-derived exosomes may be an important carrier of α-synuclein (α-syn), which induces neurodegeneration and neuronal apoptosis (Guo et al., 2020; Pinnell et al., 2021). Our earlier results indicated that microglial exosomes are key participants in PD progression in PQ-impaired environments. Activated microglia secrete a large number of exosomes that specifically carry microRNAs (miRNAs) involved in neurodegeneration. Dopaminergic neurons internalize these exosomes, which aggravate the changes in neuronal function (unpublished data).

Circular RNAs (circRNAs) are associated with several neurodegenerative diseases and may play an important role in the diagnosis and pathophysiological processes (Feng et al., 2020; Floris et al., 2017). Previously, we reported that circRNA expression is altered in a PD model of Neuro-2a cells treated with PQ (Chen et al., 2021). CircRNAs can adsorb downstream miRNAs like a "sponge" and can be used as competitive endogenous mRNA to modulate the degree of miRNAs in target genes (Li et al., 2018). CircRNAs are responsible for "the regulation of miRNA on downstream mRNA" and remove "the inhibition of miRNA on downstream mRNA" (Kristensen et al., 2019; Panda, 2018; Yang et al., 2022). The combination of miRNAs and mRNA can reduce mRNA translation, whereas the competitive combination of circRNAs with miRNAs can restore or improve mRNA translation (Kristensen et al., 2019; Yang et al., 2022). Competitive endogenous RNA (ceRNA) can be used by ceRNA molecules (mRNA, circRNA, pseudogenes, etc.) to compete with the same miRNA with the same miRNA response element (MRE) to achieve a level of adjustment to each other (Chan and Tay, 2018; Salmena et al., 2011). CeRNA, which is a circRNA-miRNA-mRNA, competes with each other to combine the common miRNA through the common MRE, and uses the miRNA bridge to affect each other to reduce miRNA inhibition or degradation, and jointly regulates gene transcription and expression in the body (Yang et al., 2018; Zeng et al., 2018). However, the roles of circRNAs in the etiopathogenesis of PD and other neurodegenerative diseases remain unclear. Additionally, whether microglial exosomes participate in neurodegenerative changes by carrying circRNAs remains unknown.

Here, we report that activated microglia-derived exosomes carrying circZNRF1 alleviated dopaminergic neuronal damage in a PQ-damaged environment by regulating miR-17–5p and Bcl2/Bax. These results provide evidence of the communication between microglia and dopaminergic neuronal cells, in which the exosome circZNRF1-mediated molecular sponge mechanism of miR-17–5p affects target cell functions. Therefore, the above studies revealed a new mechanism underlying neurodegenerative changes.

2. Materials and methods

2.1. Cell culture and PQ exposure

Mouse microglial cells (BV2, were donated by the Fujian Medical University Key Laboratory of Brain Aging and Neurodegenerative Diseases (Fuzhou, China)) and mouse dopaminergic neuron cells (MN9D, were donated by Dr. Mao from Southern Medical University (Guangzhou, China)) were selected for intercellular communication between microglia and neuronal cells, neurodegeneration, and PD, based on our earlier study (Zhang et al., 2021). Cells were prepared in a high glucose Dulbecco's modified Eagle medium (DMEM) (Gibco, USA) containing 1 % penicillin-streptomycin (Gibco, USA) and 10 % fetal bovine serum (FBS) (HyClone, USA) cultured under a constant temperature and in a humidity incubator at 37 °C and 95 % air/5 % CO_2 (Zhan et al., 2020).

PQ was purchased from Sigma-Aldrich (St. Louis, MO, USA). FBS was also prepared via ultracentrifugation at 100,000×*g* for more than 18 h to obtain vesicle-depleted FBS, thus ensuring no bovine extracellular vesicle contamination in the FBS (Mondal et al., 2019). Simultaneously, BV2 and MN9D cells were treated with 40 and 100 μM PQ, respectively, for 24 h, according to the cell viability results (Fig. S1 A-B). BV2 cells were treated with PQ at two dosages (0 and 40 μM PQ) for 24 h to obtain a supernatant containing cells secreting exosomes from the control group (Ctrl-EXOs) and PQ group (PQ-EXOs). MN9D cells were pre-incubated with 1×10^7 particle exosomes per dish for 12 h, and the MN9D cells were subsequently treated with 100 μM PQ for 24 h to establish effective exosome incubation of the *in vitro* PD model.

2.2. Exosome isolation

We collected the culture supernatant of BV2 cells using the above culture conditions, and gradient centrifuged the supernatant at 4 °C according to the steps in Fig. 1A. Obtained exosomes were resuspended in phosphate buffered saline (PBS) (Biosharp, China) and stored at − 80 °C (Li et al., 2017).

2.3. Detection of exosome characterization

Briefly, 5 μL of the exosome suspension was removed, placed on a 2 mm-diameter copper mesh (Zhongjingkeyi, China), and allowed to settle for 1 min. The filter paper absorbed the floating liquid. The sample side of the copper mesh was covered with 10 μL of 2 % phosphotungstic acid solution (Zhongjingkeyi, China), negatively stained for 5 min, placed on the copper mesh with filter paper to absorb the floating liquid, and dried for a few minutes at 25 °C. Electron microscopy imaging was performed at 80 kV and transmission electron microscopy (TEM) (FEI, USA) images were obtained. Nanoparticle tracking analysis (NTA) service was provided by VivaCell (Shanghai, China). The ZetaView PMX 110 (Particle Metrix, Germany) was used to measure the exosome concentration and particle size.

2.4. Western blot analysis

Exosome and cell total protein samples were first extracted using 0.1 % (vol/vol) PMSF in lysis buffer (Phygene, China) and denatured at 95 °C with loading buffer. For details on the electrophoresis and electroblotted protocol, see (Zheng et al., 2021). The antibodies used are found in Supplementary Materials Table S1.

2.5. Sequencing library preparation and circRNA sequencing analysis

We selected 0 and 40 μM PQ exposed BV2 exosomes for circular RNA sequencing (circRNA-seq). Briefly, the total RNA of the exosomes was extracted and rRNA was removed. Second, quality control and quantification of the RNA library were performed. An Illumina Novaseq 6000 (Illumina, USA) instrument was used for sequencing, and Q30 was used

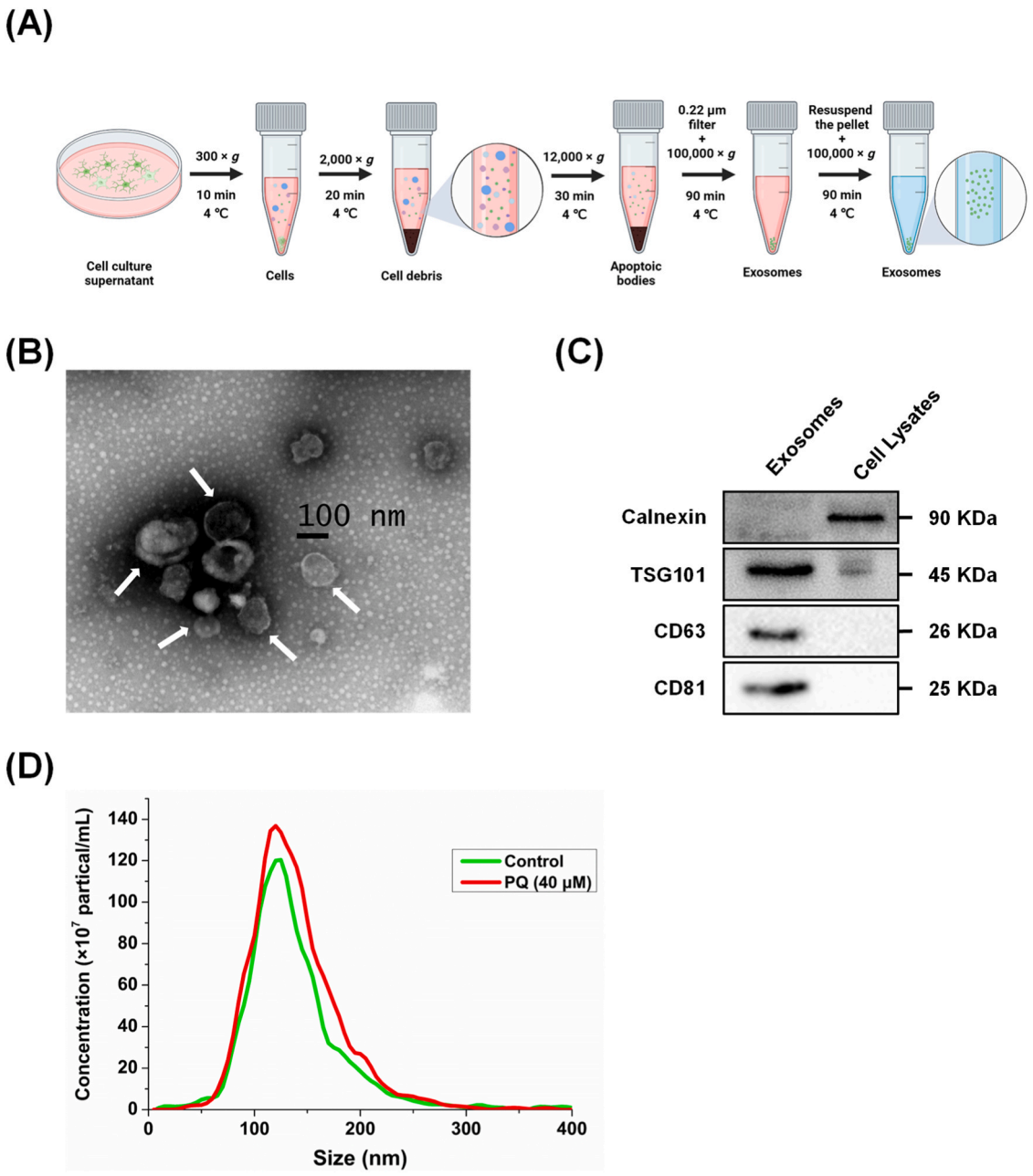

Fig. 1. Characterization of BV2 cellular exosomes. (A) Schematic diagram of exosome extraction. (B) TEM image of exosomes. White arrows indicate exosomes. Scale bar, 100 nm. (C) Western blotting analysis of exosome marker proteins TSG101, CD63, CD81 and negative control protein Calnexin. (D) Particle size and quantification of exosomes by NTA.

for quality control (Lopez-Jimenez et al., 2018). Finally, we standardized the data and analyzed the differential expression of circRNAs.

2.6. Predicting miRNA binding sites of circRNAs

We used the experimental scheme reported by (Xu et al., 2019) to predict the miRNA-binding sites of circRNAs. Briefly, we used prediction software, such as miRanda (https://mirdb.org/) and TargetScan (https://www.targetscan.org/), to predict the target of circRNA, and subsequently screened the top five miRNAs to build an interaction network using Cytoscape software (version 3.7.2; NIH, USA).

2.7. RNA isolation and qRT-PCR

The Trizol reagent (Takara, Japan) was used to extract total RNA from cells and exosomes. For circRNAs, total RNA was treated with RNasR (GENESEED, China) to remove linear RNA species (Peng et al., 2021). RNA was synthesized into cDNA using a reverse transcription kit (AG, China). Thereafter, the cDNA samples were amplified using a qPCR kit, and circRNA (AG, China) and miRNA (Takara, Japan) levels were normalized to those of *GAPDH* and *U6* snRNA. RNA expression was detected using a QuantStudio® Q5 (ABI, USA). The reaction conditions were as follows: 37 °C for 15 min, and 50 cycles at 95 °C for 30 s and 55 °C for 34 s. The expression levels were calculated using the $2^{-\Delta\Delta Ct}$ method (Bubner and Baldwin, 2004). The kits are shown in Supplementary Materials Table S2, and the primers are shown in Supplementary Materials Table S3.

2.8. Bioinformatics analysis

To generate a profile of differentially expressed circRNAs between 0 and 40 μM PQ exosomes, clustering analysis of differentially expressed circular RNAs with normalized reads using the heatmap2 package for R was performed based on the degree of all identified circRNAs and the significant differences between the two groups. Gene ontology (GO) analysis was performed to predict potential functions, including cellular components, molecular functions, and biological processes, using the source genes of the differentially expressed circRNAs (Sherman et al., 2022). Kyoto Encyclopedia of Genes and Genomes (KEGG) pathway annotations were based on pathway analysis of differentially expressed circRNA-derived genes; the pathways in which they were involved and their biological functions were inferred (Kanehisa et al., 2017).

2.9. Flow cytometry

We used the Annexin V Apoptosis Detection Kit (BD, USA) to detect apoptosis. Briefly, the cells were centrifuged at 500×*g* for 8 min to separate cultured MN9D cells. Thereafter, 100 μL binding buffer was added to each tube to resuspend the cells; 5 μL 7-AAD labeled Annexin-V dye and 5 μL PI dye was added at 25 °C for 15 min in the dark. Last, 100 μL binding buffer was added to each tube, and the test was performed within 1 h.

To detect reactive oxygen species (ROS), we used the ROS Assay Kit (Beyotime, China). A group of cell samples was used as a positive control, and Rosup solution was added in advance for 20 min. Briefly, the cells were centrifuged at 500×*g* for 8 min to separate the cultured MN9D cells and subsequently washed twice with DMEM. Thereafter, the DCFH-DA dye was dissolved in DMEM at a ratio of 1:1000 to resuspend the cells. Finally, the sample was incubated at 37 °C for 20 min and the test was performed within 1 h. The FACSCanto™ II flow cytometer (BD, USA) was used for detection.

2.10. MicroRNA antagomir transfection

MiR-17–5p antagomir and miRNA inhibitor negative controls were provided by GenePharma Co., Ltd. (Shanghai, China). Sequences are listed in Supplementary Materials Table S4. The Lipo2000 transfection reagent (Thermo Fisher Scientific, USA) was used to transfect BV2 cells with 75 nM miR-17–5p antagomir (diluted in Lipo2000 transfection reagent) and miRNA inhibitor negative control in Opti-MEM medium (Gibco, USA).

2.11. Statistical analyses

All data were analyzed using SPSS software (version 20.0; IBM, USA). Differences between groups were analyzed using one-way analysis of variance. If the *F* values were significant, the least significant difference post hoc test was used to compare multiple groups. Results are expressed as the mean ± SEM, and $P < 0.05$ was considered a significant difference.

3. Results

3.1. Morphological identification, particle size, and quantitative analysis of exosomes derived from BV2 cells

To study the exosomes secreted by BV2 cells, we used gradient centrifugation to separate and purify the exosomes from the culture supernatant of microglial cells (Fig. 1A), and used TEM and NTA to understand the morphology and size distribution of the exosomes. The TEM results showed that the vesicles of the purified exosome samples were approximately 100 nm in diameter and had typical double-membrane saucer-like and spherical shapes (Fig. 1B). We further verified the existence of the exosome marker proteins TSG101, CD63, and CD81, and the negative marker protein calnexin (Fig. 1C). In addition, NTA showed that the size of exosomes ranged from 50 to 200 nm, and the cell supernatant had approximately 1.6×10^{10} particles/mL (Fig. 1D), and it was also demonstrated that exosome secretion increased after PQ exposure.

3.2. BV2 cell-derived exosomes alleviate neurodegenerative damage and apoptosis in PQ-treated MN9D cells

Apoptosis of dopaminergic neurons in the substantia nigra striatum, which leads to their loss, is the primary mechanism of PD (Liu et al., 2022; Tompkins et al., 1997). In this study, we constructed an *in vitro* PD model using PQ-treated MN9D cells and explored the effects of BV2 cell-derived exosomes on apoptosis of this model. The results showed that after MN9D cells (without PQ-treated, control group) received PQ-EXOs, the expression of the apoptosis pathway proteins cleaved-caspase 3 and 9 was upregulated. The total level of apoptosis-related proteins was also tested; however, the pro-caspase 3 and 9 proteins also showed the same trend as the post-splicing protein under this culture model (Fig. 2A–F). The apoptotic protein Bax increased, and the anti-apoptotic protein Bcl2 decreased (Fig. 2G–I). Simultaneously, we found that BV2 cell-derived exosomes had different effects on PQ-treated MN9D cell apoptotic proteins, causing the expression of Bax, pro-caspase 3 and 9, and cleaved-caspase 3 and 9. We also simultaneously detected the expression of Bcl2 in BV2 cells treated with PQ (Fig. S2 A-B), and the relative expression of *Bcl2* mRNA in BV2 cells and exosomes (Fig. S2 C-D). The results showed no significant difference in the mRNA or protein levels between the PQ treatment and control groups. Apoptosis is a complex biochemical process involving several factors. Therefore, we analyzed the Bcl2/Bax ratio and found that in the PQ exposure group, PQ-EXOs reversed the apoptosis-promoting effect of cells exposed to PQ. However, in the control group, PQ-EXOs played the opposite role (Fig. 2J). For further verification, we used flow cytometry to detect apoptotic cells and found that when MN9D cells were treated with PQ, the number of apoptotic cells increased significantly ($P < 0.001$), and PQ-EXOs alleviated apoptosis caused by PQ-treated cells (Fig. 2K-L). Thus, we found that when MN9D cells mimic PD-like pathological symptoms, exosomes reduce the increase in apoptosis caused by PQ exposure.

3.3. BV2 cell-derived exosomes reduce the ROS level of neurons and alleviate apoptosis in PQ-treated MN9D cells

Typically, ROS levels increase after PQ exposure and impair the permeability of mitochondrial membranes inducing cell death (Huang et al., 2016). In this study, we investigated whether the effect of BV2 cell-derived exosomes on the apoptosis of MN9D cells is related to changes in intracellular ROS. The results showed that the level of ROS in BV2 cells significantly increased ($P < 0.05$) after PQ treatment for 24 h; however, there was no dose-dependent effect (Fig. 3A-B). We further detected ROS levels in the PQ-EXO incubation model and found that exosome incubation reduced the ROS levels of PQ-treated MN9D cells, indicating that PQ-EXOs slow down apoptosis. However, for normal MN9D cells, the exosomes of BV2 cells did not reduce their ROS levels (Fig. 3C).

3.4. Alterations of the circRNA expression profiles of BV2 cell-derived exosomes after PQ treatment

After exposure of BV2 cells to 0 and 40 μM PQ, purified exosome samples were extracted and analyzed using circRNA-seq to study the expression profiles of differential circRNAs in exosomes. Most of these dysregulated circRNAs were exons, followed by sense-overlapping circRNAs (Fig. 4A). In total, 113 differentially expressed circRNAs were identified ($P < 0.05$), of which 49 were upregulated (red) and 64 were downregulated (blue) (Fig. 4B). Furthermore, compared to the

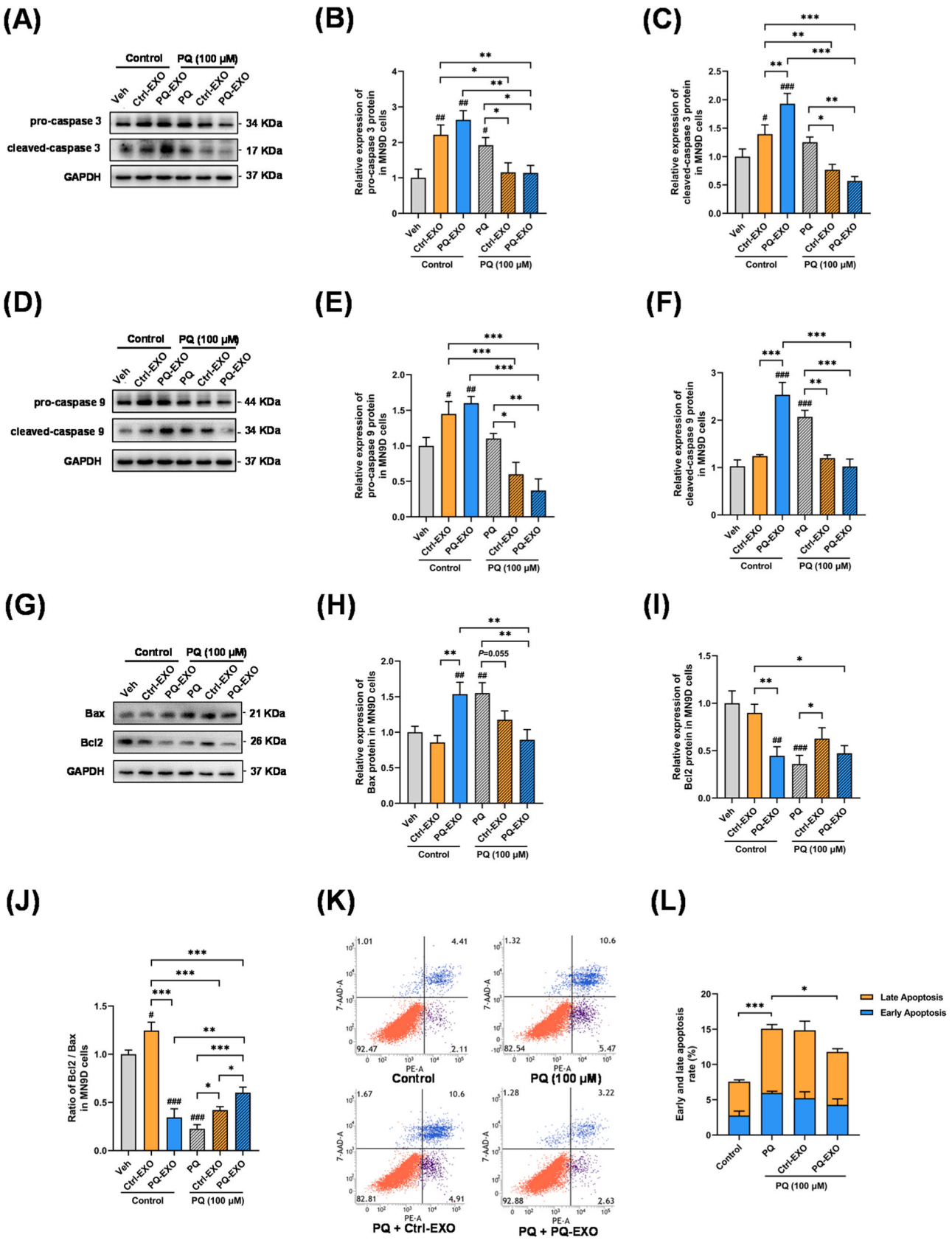

Fig. 2. Effects of BV2 cell-derived exosomes on the apoptosis level of *in vitro* PQ exposure PD model. (Veh: Vehicle control; Ctrl+EXO:Control exosome; PQ+EXO: 40 μM PQ treated exosome.)(A-I) Western blotting analysis of pro-caspase 3, cleaved-caspase 3, pro-caspase 9, cleaved-caspase 9 and Bax, Bcl2 proteins. (J) The ratio of Bcl2/Bax was shown by statistical chart. (K-L). The degree of apoptosis detected by flow cytometry. Data are shown as mean ± SEM (n = 3); # $P < 0.05$, ## $P < 0.01$, ### $P < 0.001$ represents compared with the Veh group; *$P < 0.05$, **$P < 0.01$, ***$P < 0.001$.

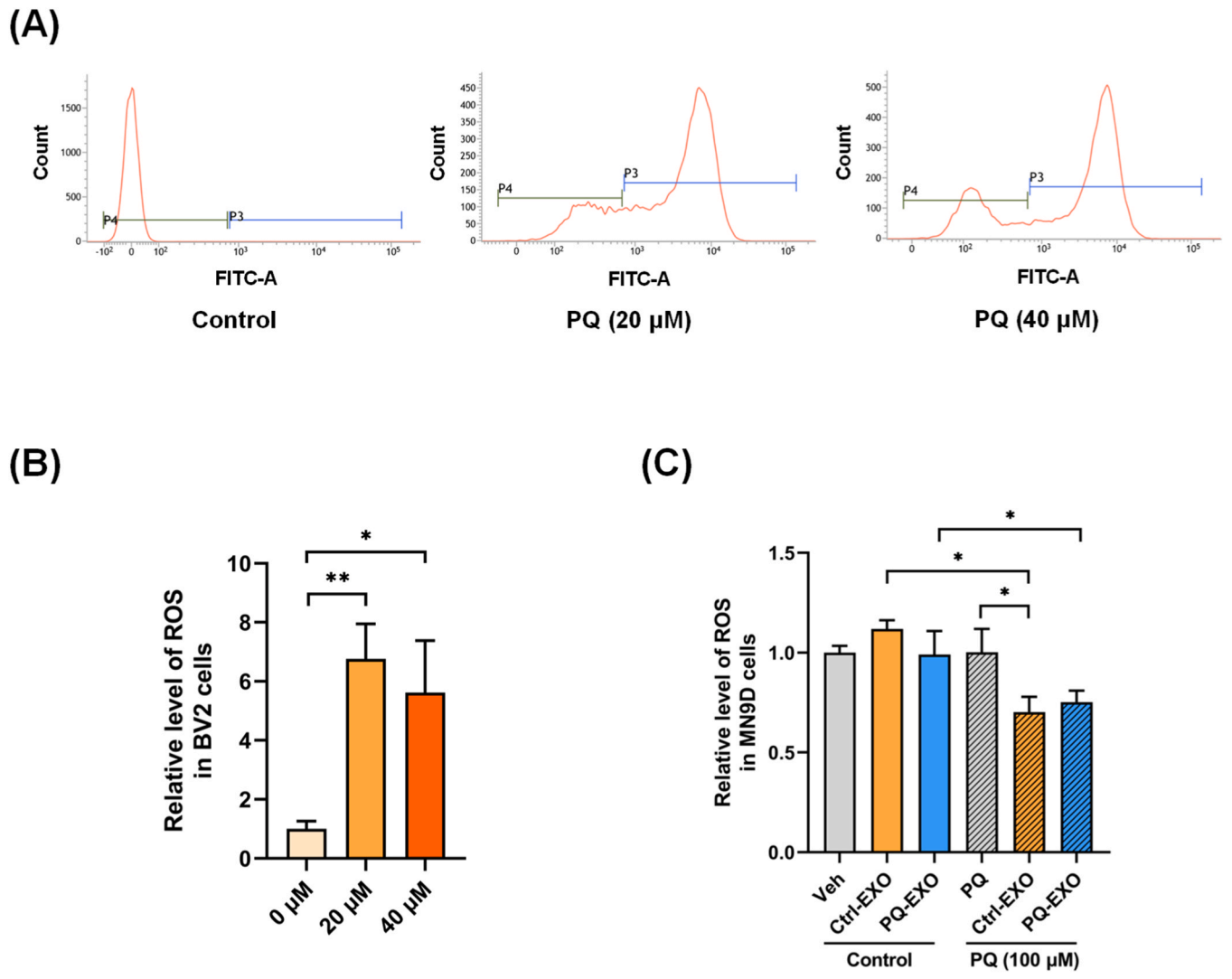

Fig. 3. The role of BV2 cell-derived exosomes on the ROS level *in vitro* PQ exposure PD model. (Veh: Vehicle control; Ctrl+EXO:Control exosome; PQ+EXO: 40 μM PQ treated exosome.) (A-B) The level of ROS in BV2 cells treated with PQ; (C) The level of ROS in MN9D cells treated with exosomes combined with PQ. Data are shown as mean ± SEM (n = 3); $^{*}P < 0.05$, $^{**}P < 0.01$.

control group, the differentially upregulated (orange) circRNAs were located on chromosomes 6, 8, 14, 15, and 16, whereas the downregulated (blue) circRNAs were primarily located on chromosomes 2, 3, 4, 7, 9, 17, 19, and X (Fig. 4C). The lengths of the differentially modified circRNAs were between 100 and 900 nt (Fig. 4D). In the cluster heatmap depicting comparison levels between the control and PQ groups, lower and higher expression levels are indicated in green and red, respectively (Fig. 4E).

GO analysis showed that these genes were primarily involved in neuronal apoptosis, neuron-neuron synaptic transmission, and cell division cycle regulation. This reflected the effects of microglial exosomes on neuronal development. Function and outcome were closely related (Fig. 4F-G). KEGG pathway enrichment analysis showed 48 signaling pathways with statistical significance, including the PI3K/AKT, Ras, AMPK, mTOR, FoxO, and neurotrophic factor signaling pathways, etc (Fig. 4H-I).

3.5. Five circRNAs enriched in the FoxO pathway are key genes for retarding apoptosis

FoxOs may mediate apoptosis, leading to the degeneration of dopaminergic neurons (Maiese, 2021). We selected the top five circRNAs enriched in the FoxO signaling pathway with the most significant differential expression for qRT-PCR verification based on KEGG pathway analysis. The results showed that circZNRF1 (circBase ID: mmu_circ_0014584) and circSTED2 (mmu_circ_0015302) were upregulated, and circCLTB (a novel circRNA), circDLGAP4 (mmu_circ_0001098), and circKIF1B (a novel circRNA) were downregulated. The expression patterns of these five circRNAs were identical to those of the circRNA-seq analysis (Fig. 5A-B). In particular, circZNRF1 expression in BV2 cells decreased after PQ exposure ($P < 0.05$), whereas its expression was reversed in exosomes ($P < 0.001$). These results suggested that circZNRF1 is selectively enriched in exosomes.

3.6. Interaction network between molecular circRNA-miRNA

Based on the above results, we selected these five differentially expressed circRNAs and used them to construct a circRNA-miRNA interactive network. Using the circBank database, we found that five circRNAs targeted 161 miRNAs. We selected the top five miRNAs among these five circRNAs for analysis, in which miR-6919–3p could be simultaneously adsorbed by two circRNAs (Fig. 6A). Notably, we found that circZNRF1 of the five adsorbed miR-17–5p, which was found in our previous study to exacerbate neurodegeneration in a model of PQ-

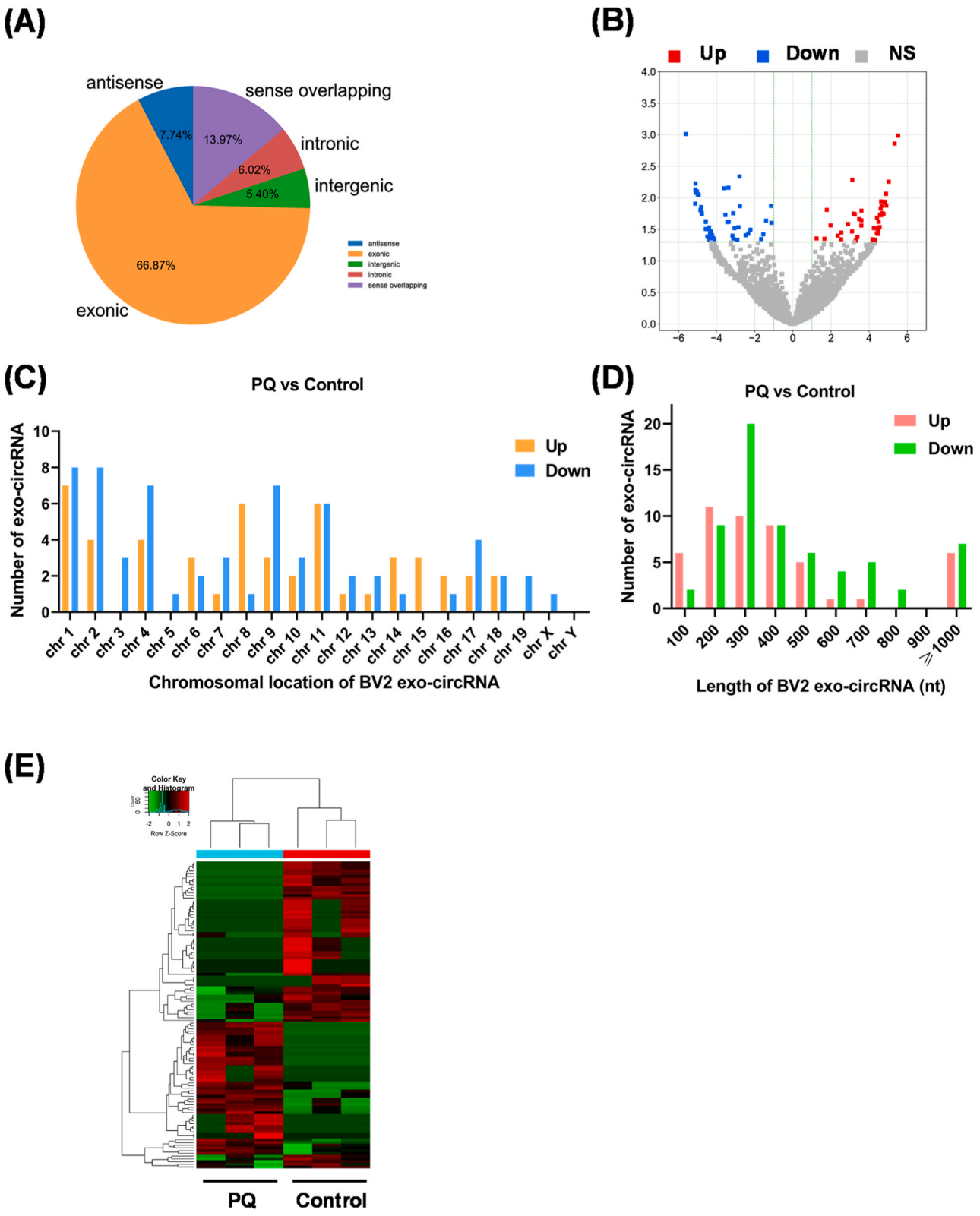

Fig. 4. Altered expression profiles of circRNAs in exosomes from BV2 cells with or without PQ exposure. (Control: Control exosome; PQ: 40 μM PQ treated exosome.) (A) Pie chart depicting the composition of circRNAs in PQ compared to control. (B) Volcano plots depicting upregulation (red) and downregulation (blue) of circRNAs in PQ compared to control. (C-D) Number and length (nt) of differentially expressed circRNAs in different chromosomes. (E) Heatmap depicting hierarchical clustering compared between control and PQ; red represents higher expression levels, green represents lower expression levels. (F-G) The most abundant GO analysis of circRNAs that increased (F) and decreased (G) in the top 10 comparisons between PQ and control; MF: Molecular Function, CC: Cellular Component, BP: Biological Process. (H-I) Histograms and bubble charts depicting the pathway analysis of the most abundant circRNAs with increased or decreased circRNAs in the top 10 comparisons between PQ and control.

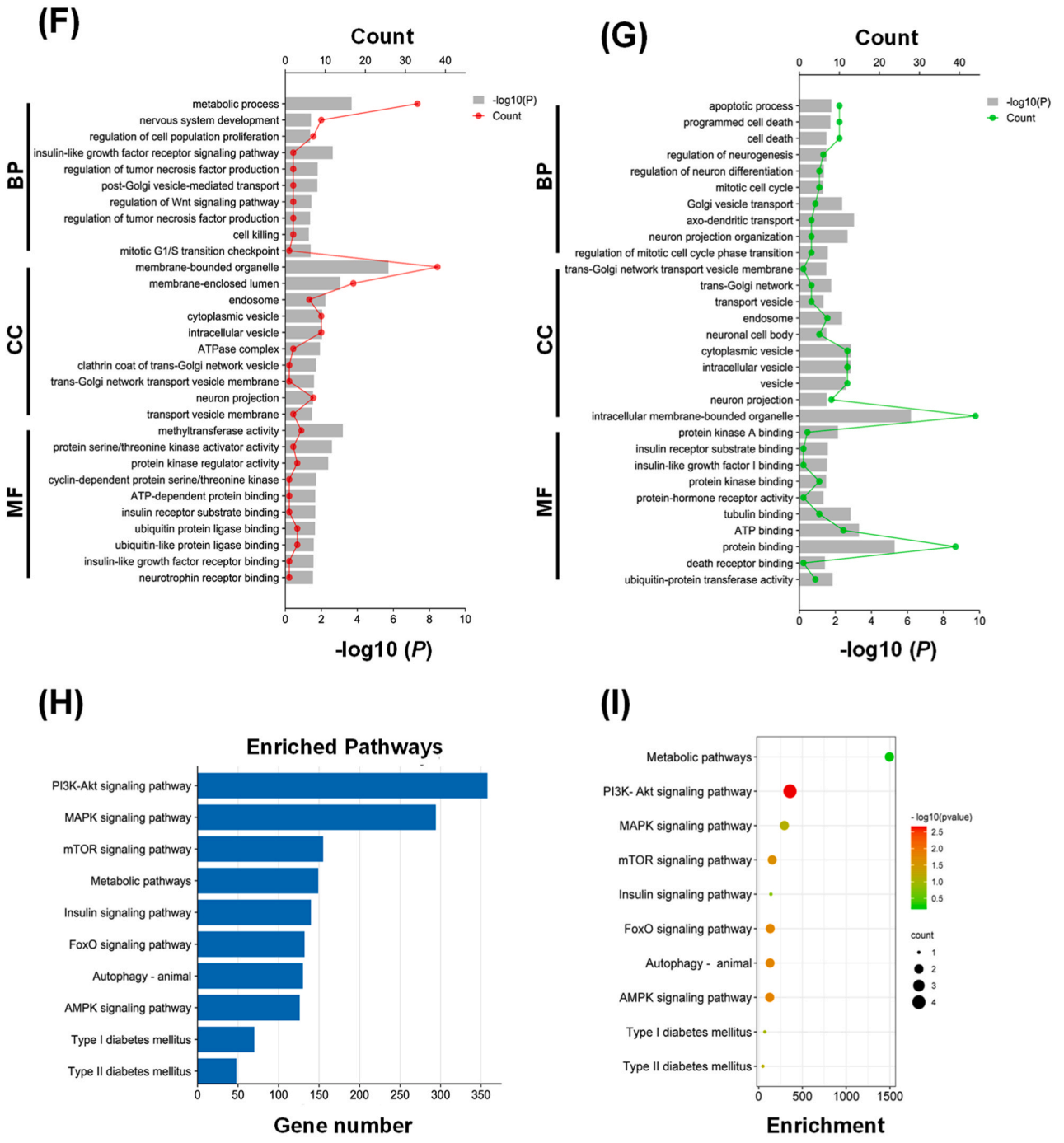

Fig. 4. (*continued*).

induced Neuro-2a cell PD damage (Wang et al., 2018). It has been confirmed that MiR-17–5p plays a crucial role in apoptosis (Kong et al., 2019). Based on these findings, we predicted the binding sites of circZNRF1 with a length of 198 bp as a sponge for miRNA adsorption to the top five miRNAs using TargetScan (Fig. 6B). We also analyzed the expression of circZNRF1 in MN9D cells (Fig. 6C). The circZNRF1 was evidently upregulated ($P < 0.05$) by PQ-EXOs in PQ-treated MN9D cells. However, the expression of circZNRF1 was not significantly altered by PQ in the absence of exosomes (PQ group compared to the vehicle group).

3.7. BV2 cell-derived exosomes participate in the biological process of PD by carrying circZNRF1 and affecting the miR-17–5p after PQ exposure in MN9D cells

CircRNAs act as miRNA sponges, adsorbing and regulating miRNAs (Li et al., 2018). We used the miRNA target gene prediction software, miRanda (Mohebbi et al., 2021), which showed that miR-17–5p may be a target of circZNRF1 in mice. This interaction was further predicted using circMIR software (Fig. 7A). Notably, our earlier study confirmed a reduction of miR-17–5p in the *in vitro* PD model exposed to PQ (Wang et al., 2018), which is consistent with our current results (Fig. 7B). We also used miRNA antagomirs on BV2 cells to obtain miR-17–5p knock-down exosomes and incubated them with MN9D cells. We used

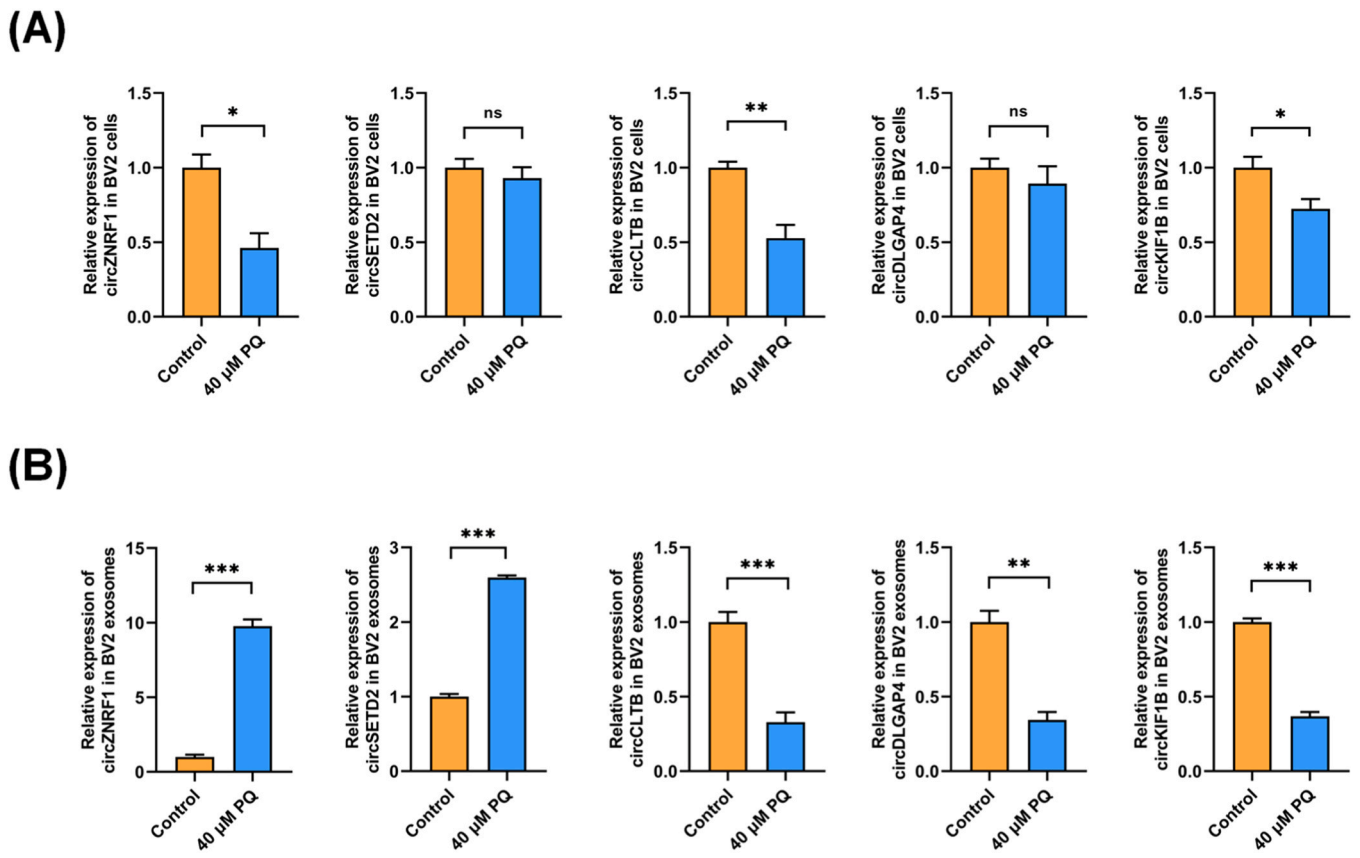

Fig. 5. Effects of PQ exposure on circRNAs expression levels in BV2 cells and exosomes. (A) Differentially expression levels of circRNAs in BV2 cells. (B) Differentially expression levels of circRNAs in BV2 cells-derived exosomes. Data are shown as mean ± SEM (n = 3); $^{*}P < 0.05$, $^{**}P < 0.01$, $^{***}P < 0.001$.

antagomirs to reduce the production of miR-17–5p in microglia, thereby reducing miR-17–5p in exosomes. This indicated that the changes in miR-17–5p in MN9D cells were not directly transmitted by exosomes. Bax expression decreased significantly ($P < 0.05$) in the presence of the miR-17–5p antagonist in PQ-EXOs; however, the expression of Bcl2 did not change significantly. Simultaneously, the Bcl2/Bax ration was also analyzed, and it was found that it was significantly increased after miR-17–5p antagomir-PQ-EXO treatment. These findings suggested that Bcl2/Bax could play an anti-apoptotic role (Fig. S3A–D). Moreover, when we reduced miR-17–5p in exosomes, changes in ROS levels were observed in MN9D cells. FACS results showed that ROS levels increased in MN9D cells treated with miR-17–5p antagomir-EXOs, and continued to increase in MN9D cells treated with miR-17–5p antagomir-PQ-EXOs (Fig. S3 E). This is consistent with previous reports that exosomes downregulate downstream target genes by delivering miR-17–5p, thereby inhibiting ROS accumulation. After the knockdown of miR-17–5p in exosomes, ROS levels increase in target cells (Ding et al., 2020). Compared to the PQ group, PQ-EXO carried a larger amount of circZNRF1 and dynamically adsorbed a larger amount of miR-17–5p, which affected the biological effects of downstream mRNAs (Fig. 7B). Notably, miR-17–5p was upregulated in the PQ-EXOs, in our miRNA-seq analysis, which was consistent with the changes in circRNAs. Furthermore, we verified that the anti-apoptotic gene *Bcl2* is a downstream target of miR-17–5p in mice (Fig. 7C). We verified that the exosomes upregulated *Bcl2* expression in MN9D cells in the presence of PQ (Fig. 7D). Furthermore, this also demonstrated that the protein level of Bcl2 varied with its mRNA levels in MN9D cells (Fig. 2A and C). Simultaneously, the production of the inflammatory cytokine IL-6 in PQ-treated BV2 cells was also detected. PQ treatment significantly increased ($P < 0.05$) the level of IL-6 in BV2 cells, whereas the miR-17–5p antagonist did not alleviate or aggravate the changes in IL-6 protein levels (Fig. S4 A-B). The above results revealed that *Bcl2* is the target of miR-17–5p, and the secretion carrying a large amount of circZNRF1 could dynamically adsorb miR-17–5p, thereby regulating the function of miR-17–5p, increasing the expression of Bcl2/Bax and alleviating the apoptotic effect under PQ exposure. This indicated that circZNRF1 is involved in the biological processes of PD through miR-17–5p. Therefore, we concluded that circZNRF1 is involved in the biological processes of PD through the miR-17–5p pathway.

4. Discussion

Recently, the function of glial cells in PD has become a focus of research (Iovino et al., 2020). Microglia are conspicuously activated in the striatum and substantia nigra of patients with PD, suggesting that they play an important role in the pathological process of PD (Cheng et al., 2020; Du et al., 2018; Shi et al., 2019). Our previous study showed that exosomes released by BV2 cells under PQ exposure alter PD-related injury manifestations in MN9D cells and affect neuronal degenerative processes (unpublished data).

We further investigated the effect of BV2 cell-derived exosomes on the level of apoptosis in an *in vitro* PD model to simulate the pathological characteristics of dopaminergic neuronal apoptosis during PD progression. Bcl2 exerts an anti-apoptotic effect by antagonizing Bax and the Bcl2/Bax ratio regulates the extent of apoptosis (Zhao et al., 2018). Caspase-3 is a major regulator of apoptosis (Eskandari and Eaves, 2022; Imbriani et al., 2019). It is activated by caspase-1, caspase-2, and itself. The activated caspase-3 may affect DNA replication, transcription, and damage repair. Its activation largely depends on the release of cytochrome C (Eid and El-Shitany, 2021; Jiao et al., 2020; Li et al., 2021). The Bcl2 family (including *Bcl2* and *Bax*) is the most important regulatory genes in apoptosis, and mediates cytochrome C release through

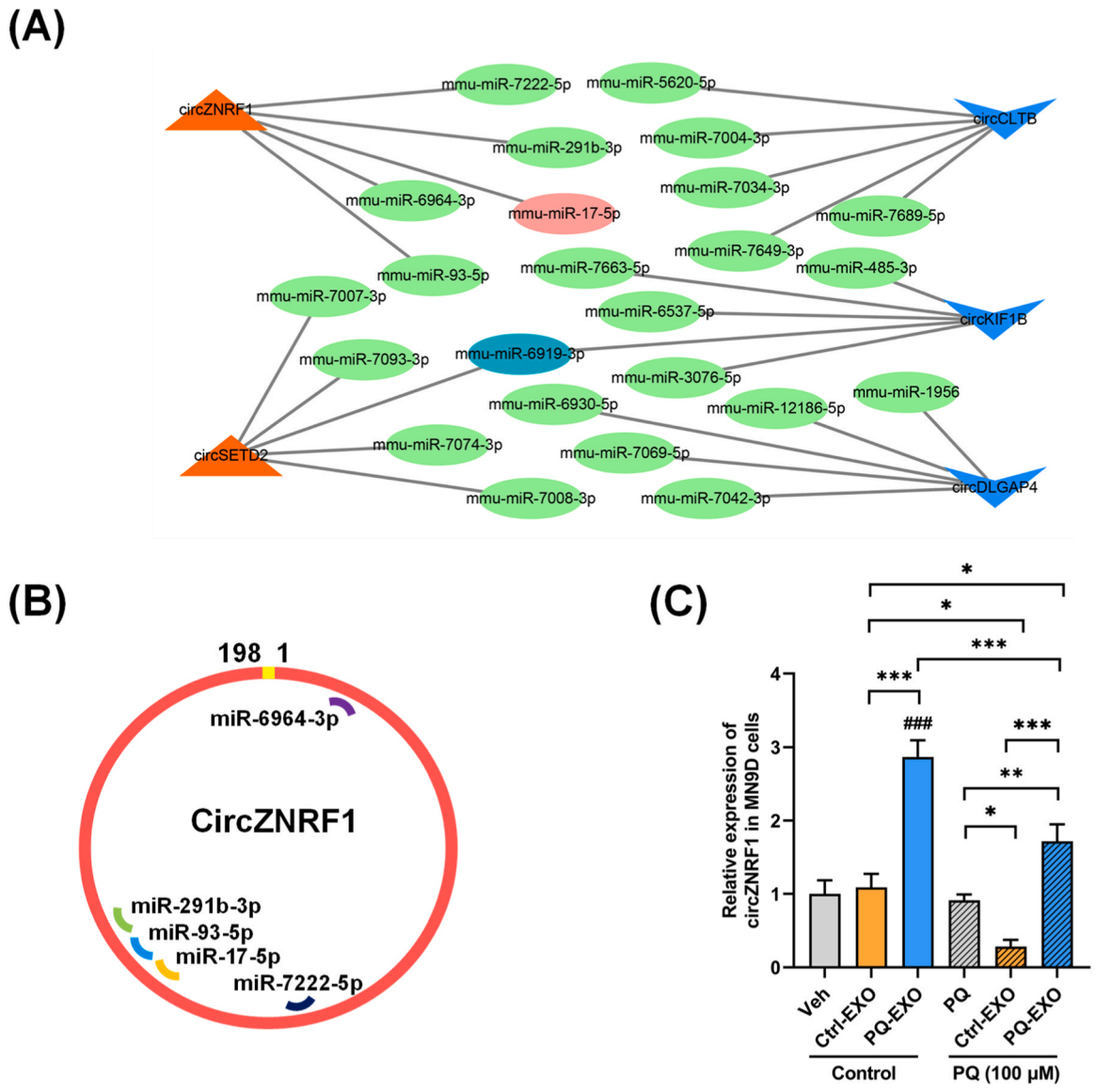

Fig. 6. Predicted circRNA-miRNA interaction analysis. (A) Interaction network map of circRNA-miRNA interaction network; (orange triangles represent up-regulated circRNAs, green arrows represent down-regulated circRNAs, blue circles predicted the top 5 miRNAs (pink circles indicate miR-17–5p)). (B) Binding sites between circZNRF1 and top 5 miRNAs. (C) Differential expression of circZNRF1 in MN9D cells treated with exosomes combined with PQ. Data are shown as mean ± SEM (n = 3); ### $P < 0.001$ compared with the Veh group; *$P < 0.05$, **$P < 0.01$, ***$P < 0.001$.

the mitochondrial pathway. Bcl2 and Bax act as upstream regulators of caspase-3 and also activate caspase-3 by recruiting pro-caspase 9 and initiating the caspase cascade (Li et al., 2021; Spitz and Gavathiotis, 2022). It can also act downstream of caspase-3 as its direct substrate and cleave itself into a fragment with Bax-like proapoptotic activity, accelerating apoptosis. In cell apoptosis, they are related to and are restricted to each other.

In our study, exosomes increased apoptosis in MN9D cells under physiological conditions. These results showed that the expression of Bcl2 decreased and that of Bax increased in MN9D cells (without PQ-treated, control group) which received PQ-EXOs. The expression of apoptotic pathway proteins cleaved-caspase 3 and 9 was also upregulated, and the total level of apoptosis-related proteins was also tested; however, the pro-caspase 3 and 9 proteins showed the same trend as the post-splicing proteins in this culture model. Notably, exosomes attenuated the apoptosis induced by PQ exposure in the *in vitro* PD model. This was further demonstrated by the fact that BV2 cell-derived exosomes had distinct effects on PQ-treated MN9D cell apoptotic proteins, resulting in the decreased expression of Bax, pro-caspase 3 and 9, and cleaved-caspase 3 and 9. Based on the Bcl2/Bax ratio, we found that in the control group, Ctrl-EXOs played an anti-apoptotic role, whereas PQ-EXOs played the opposite role. In the PQ exposure group, PQ-EXOs reversed the apoptosis-promoting effect of PQ. We calculated the ratio of Bcl2/Bax to evaluate the anti-apoptotic effects of Ctrl-EXOs and PQ-EXOs and found that PQ-EXOs were more effective. These results suggested that PQ-EXOs play an anti-apoptotic role in the PQ-exposed environment. Notably, microglial exosomes played a completely different role in the control and PQ-treated MN9D cells. In addition to the Bcl2/Bax ratio, we examined the proliferative activity of dopaminergic neuronal cells and some PD-associated proteins (α-syn, Parkin, PINK1, TH, and p-TH [Ser40] proteins) (unpublished data). These results confirmed this phenomenon. This suggested that the influence of the recipient cell environment was greater than that of the donor substrate in some cases. In addition, we found that PQ-EXOs reduced ROS levels in MN9D cells exposed to PQ. This was similar to the results of our previous study, where PQ exposure led to an increase in ROS in Neuro-2a cells, resulting in the downregulation of miR-17–5p expression and promotion of apoptosis. Reactive oxygen scavengers can reduce PQ-

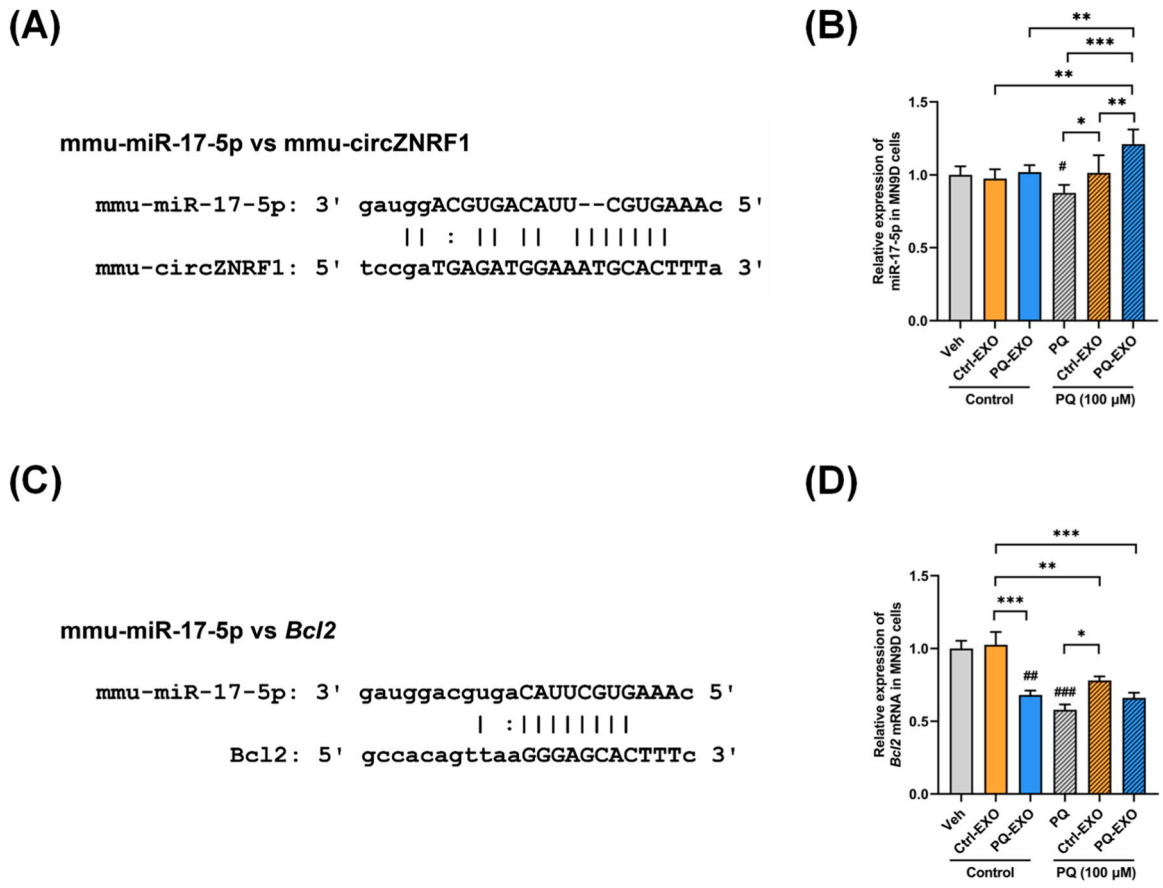

Fig. 7. BV2 cells-derived exosomes carried circZNRF1 and affected the miR-17–5p/Bcl2 *in vitro* PQ exposure PD model. (Veh: Vehicle control; Ctrl+EXO:Control exosome; PQ+EXO: 40 μM PQ treated exosome.)(A)Predicted the corresponding target sequence sites of miR-17–5p on circZNRF1. (B) Validation of the changes in the expression level of miR-17–5p in MN9D cells by PQ treatment in the exosome incubation model. (C) Predicted target sequences of miR-17–5p and *Bcl2* at corresponding sites. (D) Validation of changes in *Bcl2* expression levels in MN9D cells by PQ treatment in an exosome incubation model. Data are shown as mean ± SEM (n = 3); # $P < 0.05$, ## $P < 0.01$, ### $P < 0.001$ compared with the Veh group; *$P < 0.05$, **$P < 0.01$, ***$P < 0.001$.

induced ROS and upregulate miR-17–5p, thereby preventing the apoptosis-promoting effect of PQ (Zhan et al., 2020).

Therefore, we aimed to determine the substances in microglia-derived exosomes that exert this effect. We found that circZNRF1 expression was elevated in the exosomes of BV2 cells after PQ exposure. In the PQ-EXO group, circZNRF1 alleviated apoptosis, thereby reducing PQ neurovirulence in MN9D cells. Therefore, we hypothesized that circZNRF1 acts as a cytoprotective factor that mitigates neuronal damage. In our study, circZNRF1 was identified as a miR-17–5p sponge and was found to be involved in the biological processes of PD via miR-17–5p in mouse cells. CircZNRF1 is a functional molecule that can adsorb miR-17–5p rather than degrade miR-17–5p; therefore, the level of miR-17–5p detected in MN9D cells was not affected by PQ-EXOs despite the high expression of circZNRF1. In the MN9D cell control group, the changes in miR-17–5p expression were not consistent with those in the PQ group, and the final functions were also different (pro-apoptotic in the control group and anti-apoptotic in the PQ group). Both miR-17–5p and circZNRF1 were highly expressed in the PQ group. Microglial exosomes played completely different roles in control and PQ-treated MN9D cells. We speculated that this difference is due to the different reaction states of MN9D cells after PQ treatment. Consistent with our previous study, miR-17–5p was downregulated in Neuro-2a cells after PQ exposure and the miR-17–5p mimic boosted cell proliferation and inhibited apoptosis (Wang et al., 2018). When MN9D cells were treated with miR-17–5p antagomir-PQ-EXOs, Bax expression significantly decreased; however, the expression of Bcl2 remained unchanged. The Bcl2/Bax ratio increased significantly compared to that in the group without exosomes. The circZNRF1 in the exosomes adsorbed miR-17–5p in MN9D cells; however, the miR-17–5p in the exosomes did not occupy the adsorption site of circZNRF1. Therefore, most of the miR-17–5p in MN9D cells was recruited by circZNRF1, and the function of the downstream Bcl2 recovered and increased, showing an anti-apoptotic effect. In contrast, the expression of the pro-inflammatory factor IL-6, which increased significantly after PQ treatment, was not affected by the miR-17–5p antagomir. This suggested that miR-17–5p is not a factor regulating inflammation and is a neurovirulence factor involved in the etiopathogenesis of certain neurodegenerative disorders.

Reduced expression of miR-17–5p suppresses cell proliferation and promotes apoptosis (Shi et al., 2020). Simultaneously, we found that miR-17–5p was upregulated in the PQ-EXO group, which may be because PQ-EXOs carried more circZNRF1 to dynamically adsorb miR-17–5p and slow the onset of PD. Using miRNA-seq, we found that miR-17–5p expression was upregulated in exosomes after PQ exposure. MiR-17–5p can regulate the expression of Bcl2, and the upregulation of miR-17–5p can improve cell function by reducing apoptosis (Ramesh et al., 2021; Saadat et al., 2020). In addition, our results indicated that the exposure of MN9D cells to PQ can reduce ROS levels after receiving exosomes, which could upregulate the expression of miR-17–5p. *Bcl2* is a target of miR-17–5p, and circZNRF1 acts as a miRNA sponge to regulate miR-17–5p, thus acting on Bcl2/Bax to play an anti-apoptotic neuroprotective role. These results indicated that the circZNRF1/miR-17–5p pathway regulates the biological process of PD by influencing the transcription of downstream genes.

5. Conclusion

In conclusion, we explored a new model of exosomes involved in microglia-neuron communication in an *in vitro* PD injury model and revealed that microglial exosomes alleviate the degeneration of dopaminergic neurons. After PQ activation of microglia, it increased its exosome number and composition, and the key molecules and specific action mechanisms between microglia and neurons. However, further studies are required to reveal the role of neuroinflammatory cell exosomes in neurodegeneration. We proposed, for the first time, that the increase in circZNRF1 transmitted by activated microglia is a self-rescue response that ameliorates PQ-mediated neuronal apoptosis. The circZNRF1/miR-17–5p pathway may be a molecular mechanism underlying the etiopathogenesis of PD and a promising target for PD therapy in the future.

CRediT authorship contribution statement

Wenya Shao: Conceptualization, Supervision, Project administration, Writing – review & editing. **Huangyuan Li:** Conceptualization, Supervision, Project administration, Writing – review & editing. **Xu Liu:** Writing – original draft, Project administration, Investigation, Writing – review & editing. **Jingwen Wu:** Investigation, Data curation. **Qingqing Wu:** Investigation, Data curation. **Fuli Zheng:** Writing – review & editing. **Guangxia Yu:** Writing – review & editing. **Jianxi Liu:** Writing – review & editing. **Zhenkun Guo:** Visualization. **Hong Hu:** Visualization. **Siying Wu:** Visualization.

Declaration of Competing Interest

The authors declare that they have no known competing financial interests or personal relationships that could have appeared to influence the work reported in this paper.

Data Availability

Data will be made available on request.

Acknowledgements

We thank members of our laboratory for helpful discussion. Our work was supported by the Provincial Natural Science Foundation of Fujian Province, China (No. 2020J01641), Startup Fund for Scientific Research, Fujian Medical University, China (No. XRCZX2018018), and National Natural Science Foundation of China (No. 81903352). The authors would like to thank the Public Technology Service Center (Fujian Medical University) for their technical assistance as well as Cloud-Seq Biotech Ltd. Co. (Shanghai, China) for the RNA high throughput sequencing service and the subsequent bioinformatics analysis. We also thank the figures were plotted by SRplot (www.bioinformatics.com.cn/srplot), on online data visualization platform (last accessed on 2 Dec, 2022).

Appendix A. Supporting information

Supplementary data associated with this article can be found in the online version at doi:10.1016/j.ecoenv.2023.115356.

References

Ahmed, H., et al., 2017. Parkinson's disease and pesticides: a meta-analysis of disease connection and genetic alterations. Biomed. Pharmacother. 90, 638–649.
Bliederhaeuser, C., et al., 2016. Age-dependent defects of alpha-synuclein oligomer uptake in microglia and monocytes. Acta Neuropathol. 131, 379–391.
Bubner, B., Baldwin, I.T., 2004. Use of real-time PCR for determining copy number and zygosity in transgenic plants. Plant Cell Rep. 23, 263–271.
Chamberlain, K.A., et al., 2021. Oligodendrocytes enhance axonal energy metabolism by deacetylation of mitochondrial proteins through transcellular delivery of SIRT2. Neuron 109, 3456-+.
Chan, J.J., Tay, Y., 2018. Noncoding RNA:RNA regulatory networks in cancer. Int. J. Mol. Sci. 19, 26.
Chen, N.Z., et al., 2021. Paraquat-induced oxidative stress regulates N6-methyladenosine (m6A) modification of circular RNAs*. Environ. Pollut. 290, 9.
Cheng, F., et al., 2020. Proinflammatory cytokines induce accumulation of glypican-1-derived heparan sulfate and the C-terminal fragment of beta-cleaved APP in autophagosomes of dividing neuronal cells. Glycobiology 30, 539–549.
Ding, C.Y., et al., 2020. Exosomal miRNA-17-5p derived from human umbilical cord mesenchymal stem cells improves ovarian function in premature ovarian insufficiency by regulating SIRT7. Stem Cells 38, 1137–1148.
Du, R.H., et al., 2018. Kir6.1/K-ATP channel modulates microglia phenotypes: implication in Parkinson's disease. Cell Death Dis. 9, 13.
Eid, B.G., El-Shitany, N.A., 2021. Captopril downregulates expression of Bax/cytochrome C/caspase-3 apoptotic pathway, reduces inflammation, and oxidative stress in cisplatin-induced acute hepatic injury. Biomed. Pharmacother. 139, 10.
Eskandari, E., Eaves, C.J., 2022. Paradoxical roles of caspase-3 in regulating cell survival, proliferation, and tumorigenesis. J. Cell Biol. 221, 13.
Fan, C.Q., et al., 2022. Microglia secrete miR-146a-5p-containing exosomes to regulate neurogenesis in depression. Mol. Ther. 30, 1300–1314.
Feng, Z., et al., 2020. Circular RNA circDLGAP4 exerts neuroprotective effects via modulating miR-134-5p/CREB pathway in Parkinson's disease. Biochem. Biophys. Res. Commun. 522, 388–394.
Floris, G., et al., 2017. Regulatory role of circular RNAs and neurological disorders. Mol. Neurobiol. 54, 5156–5165.
Guo, M., et al., 2020. Microglial exosomes facilitate alpha-synuclein transmission in Parkinson's disease. Brain 143, 1476–1497.
Huang, C.L., et al., 2016. Paraquat induces cell death through impairing mitochondrial membrane permeability. Mol. Neurobiol. 53, 2169–2188.
Huang, Y.H., et al., 2019. Paraquat degradation from contaminated environments: current achievements and perspectives. Front. Microbiol. 10, 9.
Imbriani, P., et al., 2019. Loss of non-apoptotic role of caspase-3 in the PINK1 mouse model of Parkinson's Disease. Int. J. Mol. Sci. 20, 19.
Iovino, L., et al., 2020. Glutamate-induced excitotoxicity in Parkinson's disease: the role of glial cells. J. Pharmacol. Sci. 144, 151–164.
Jiao, C.W., et al., 2020. Ganoderma lucidum spore oil induces apoptosis of breast cancer cells in vitro and in vivo by activating caspase-3 and caspase-9. J. Ethnopharmacol. 247, 9.
Kalluri, R., LeBleu, V.S., 2020. The biology, function, and biomedical applications of exosomes. Science 367, 640-+.
Kanehisa, M., et al., 2017. KEGG: new perspectives on genomes, pathways, diseases and drugs. Nucleic Acids Res. 45, D353–D361.
Kong, Y.Y., et al., 2019. Ferroportin downregulation promotes cell proliferation by modulating the Nrf2-miR-17-5p axis in multiple myeloma. Cell Death Dis. 10, 12.
Kristensen, L.S., et al., 2019. The biogenesis, biology and characterization of circular RNAs. Nat. Rev. Genet. 20, 675–691.
Li, P., et al., 2017. Progress in exosome isolation techniques. Theranostics 7, 789–804.
Li, X., et al., 2018. The biogenesis, functions, and challenges of circular RNAs. Mol. Cell 71, 428–442.
Li, Z.X., et al., 2021. A preparation of Ginkgo biloba L. leaves extract inhibits the apoptosis of hippocampal neurons in post-stroke mice via regulating the expression of Bax/Bcl-2 and Caspase-3. J. Ethnopharmacol. 280, 10.
Liu, T.W., et al., 2022. Biomarker of neuroinflammation in Parkinson's disease. Int. J. Mol. Sci. 23, 16.
Lopez-Jimenez, E., et al., 2018. RNA sequencing and prediction tools for circular RNAs analysis. In: Xiao, J. (Ed.), Circular Rnas: Biogenesis and Functions. Springer-Verlag Singapore Pte Ltd, Singapore, pp. 17–33.
Maiese, K., 2021. Targeting the core of neurodegeneration: FoxO, mTOR, and SIRT1. Neural Regen. Res. 16, 448–455.
Mohebbi, M., et al., 2021. Human MicroRNA target prediction via multi-hypotheses learning. J. Comput. Biol. 28, 117–132.
Mondal, A., et al., 2019. Effective visualization and easy tracking of extracellular vesicles in glioma cells. Biol. Proced. Online 21, 12.
Panda, A.C., 2018. Circular RNAs Act as miRNA Sponges. In: Xiao, J. (Ed.), Circular Rnas: Biogenesis and Functions. Springer-Verlag Singapore Pte Ltd, Singapore, pp. 67–79.
Peng, Y., et al., 2021. A novel protein AXIN1-295aa encoded by circAXIN1 activates the Wnt/beta-catenin signaling pathway to promote gastric cancer progression. Mol. Cancer 20, 19.
Peng, Z.L., et al., 2019. Activation of microglia synergistically enhances neurodegeneration caused by MPP+ in human SH-SY5Y cells. Eur. J. Pharmacol. 850, 64–74.
Pinnell, J.R., et al., 2021. Exosomes in Parkinson disease. J. Neurochem. 157, 413–428.
Qiao, C., et al., 2022. Targeting microglial NLRP3 in the SNc region as a promising disease-modifying therapy for Parkinson's disease. Brain Behav. 12, 10.
Ramesh, P., et al., 2021. BCL-XL is crucial for progression through the adenoma-to-carcinoma sequence of colorectal cancer. Cell Death Differ. 28, 3282–3296.
Saadat, Y.R., et al., 2020. Modulatory role of vaginal-isolated lactococcus lactis on the expression of miR-21, miR-200b, and TLR-4 in CAOV-4 cells and in silico revalidation. Probiotics Antimicrob. Proteins 12, 1083–1096.
Salmena, L., et al., 2011. A ceRNA hypothesis: the Rosetta stone of a Hidden RNA Language? Cell 146, 353–358.
Sherman, B.T., et al., 2022. DAVID: a web server for functional enrichment analysis and functional annotation of gene lists (2021 update). Nucleic Acids Res. 50, W216–W221.

Shi, Y., et al., 2019. Microglia drive APOE-dependent neurodegeneration in a tauopathy mouse model. J. Exp. Med. 216, 2546–2561.
Shi, Y.P., et al., 2020. miR-17-5p knockdown inhibits proliferation, autophagy and promotes apoptosis in thyroid cancer via targeting PTEN. Neoplasma 67, 249-+.
Spitz, A.Z., Gavathiotis, E., 2022. Physiological and pharmacological modulation of BAX. Trends Pharmacol. Sci. 43, 206–220.
Stuart, A.M., et al., 2023. Agriculture without paraquat is feasible without loss of productivity-lessons learned from phasing out a highly hazardous herbicide. Environ. Sci. Pollut. Res. 30, 16984–17008.
Tangamornsuksan, W., et al., 2019. Paraquat exposure and Parkinson's disease: a systematic review and meta-analysis. Arch. Environ. Occup. Health 74, 225–238.
Tompkins, M.M., et al., 1997. Apoptotic-like changes in Lewy-body-associated disorders and normal aging in substantia nigral neurons. Am. J. Pathol. 150, 119–131.
Verssimo, G., et al., 2017. Paraquat disrupts the anti-inflammatory action of cortisol in human macrophages in vitro: therapeutic implications for paraquat intoxications. Toxicol. Res. 6, 232–241.
Wang, Q.Q., et al., 2017. Paraquat and MPTP induce neurodegeneration and alteration in the expression profile of microRNAs: the role of transcription factor Nrf2. Npj Park. Dis. 3, 10.
Wang, Q.Q., et al., 2018. Paraquat and MPTP alter microRNA expression profiles, and downregulated expression of miR-17-5p contributes to PQ-induced dopaminergic neurodegeneration. J. Appl. Toxicol. 38, 665–677.
Xu, H.C., et al., 2019. RNA-Seq profiling of circular RNAs in human colorectal Cancer liver metastasis and the potential biomarkers. Mol. Cancer 18, 6.
Yang, C.D., et al., 2018. Circular RNA circ-ITCH inhibits bladder cancer progression by sponging miR-17/miR-224 and regulating p21, PTEN expression. Mol. Cancer 17, 12.
Yang, L., et al., 2022. Biogenesis and regulatory roles of circular RNAs. Annu. Rev. Cell Dev. Biol. 38, 263–289.
Zeng, K.X., et al., 2018. CircHIPK3 promotes colorectal cancer growth and metastasis by sponging miR-7. Cell Death Dis. 9, 15.
Zhan, Y.T., et al., 2020. Reactive oxygen species regulatemiR-17-5p expression viaDNAmethylation in paraquat-induced nerve cell damage. Environ. Toxicol. 35, 1364–1373.
Zhang, X.F., et al., 2016. Multifactorial theory applied to the neurotoxicity of paraquat and paraquat-induced mechanisms of developing Parkinson's disease. Lab. Investig. 96, 496–507.
Zhang, Y.Y., et al., 2021. Inflammatory lncRNA AK039862 regulates paraquat-inhibited proliferation and migration of microglial and neuronal cells through the Pafah1b1/Foxa1 pathway in co-culture environments. Ecotoxicol. Environ. Saf. 208, 11.
Zhao, T.F., et al., 2018. Ligustrazine suppresses neuron apoptosis via the Bax/Bcl-2 and caspase-3 pathway in PC12 cells and in rats with vascular dementia. Iubmb Life 70, 60–70.
Zheng, F.L., et al., 2021. Cobalt induces neurodegenerative damages through Pin1 inactivation in mice and human neuroglioma cells. J. Hazard. Mater. 419, 17.